
Article:
Mansfield, J.T., Thorpe, C.L. orcid.org/0000-0002-2860-8611, Corkhill, C.L. orcid.org/0000-0002-7488-3219 et al. (2 more authors) (2023) Localised extended ("vermiform") features formed during glass dissolution. Journal of Non-Crystalline Solids, 608. 122230. ISSN 0022-3093

https://doi.org/10.1016/j.jnoncrysol.2023.122230

Journal of Non-Crystalline Solids 608 (2023) 122230

Contents lists available at ScienceDirect

Journal of Non-Crystalline Solids

journal homepage: www.elsevier.com/locate/jnoncrysol

Localised extended ("vermiform") features formed during glass dissolution

James T. Mansfield [a,1], Clare L. Thorpe [a], Claire L. Corkhill [a], Mike T. Harrison [b], Russell J. Hand [a,*]

[a] Department of Materials Science & Engineering, University of Sheffield, Sir Robert Hadfield Building, Mappin Street, Sheffield S1 3JD, UK
[b] National Nuclear Laboratory, Central Laboratory, Sellafield, Seascale, Cumbria CA20 1PG, UK

A B S T R A C T

Studies on glass durability are important to our understanding of the likely long term behaviour of vitrified nuclear wastes, natural and archaeological glasses; there has, however, been little in the way of systematic reporting of features associated with localised chemical attack on such glasses. Durability experiments performed in water at 90 °C from 28 d to 672 d on glass monoliths of 5 different compositions: 3 basaltic compositions; an inactive version of the 25 wt% loaded UK mixture Windscale (MW25) glass and the International Simple Glass (ISG) all yielded locally extended or vermiform alteration features. Similar features are seen on all glasses at all dissolution times studied. The number of features and whether they were filled by alteration products or not was dependant on glass composition. The majority of features have quite simple geometries but lesser numbers of more complex morphologies are seen. The location of these features is thought to be most probably linked to residual damage arising from the monolith production providing sites for locally accelerated dissolution. Despite being sites of localised accelerated dissolution the impact of these features on the total surface area is calculated to be limited. Hence the surface area term used to calculate normalised mass losses and normalised loss rates will not be greatly in error as a result of these features.

1. Introduction

Significant work has been conducted over the last few decades on the corrosion of glasses in the context of nuclear waste disposal (see, for example, [1]). Despite the extensive nature of this work and the occasional reported observation of localised attack on laboratory samples [2–4] there has been relatively little in the way of systematic reporting of features associated with localised more accelerated attack on the glass surface for nuclear waste glasses, although such features have been reported on the surface of archaeological glasses [5,6]. The characteristic micrometre scale features generated *via* this process may influence overall dissolution rates, for example, by affecting exposed surface areas [4,7], and localised attack and gel layer formation may potentially be coupled [8] as the former provides the elements to form the latter. As part of a larger programme of glass durability testing we have identified a range of these features in multiple glasses and they are considered in detail in this paper.

2. Background

Localised attack during the corrosion of glasses has been previously been categorised in the literature as resulting in pitted surfaces and/or more extended features. While the extended features are of primary concern in this work both types of feature are reviewed below.

2.1. Pits and pitting

Pitting is frequently observed on altered archaeological glasses [5,6,9,10], natural glasses [11–13] as well as technical glasses dissolved in the laboratory [3,4,7]. In natural glasses these features have been suggested as arising from attack by micro-organisms [14,15] although the evidence for this has been disputed [16], as such features can arise from abiotic dissolution mechanisms [17] controlled by simple diffusive processes [15].

Pits associated with glass dissolution typically occur on the glass below alteration layers, if present [7,4]. Pits are approximately hemispherical, with diameters < 10 μm [4,8]; although they may be elongated with lengths up to 100 μm [8]. Pitting abundance appears to increase with dissolution duration and aggressiveness (*e.g.* high temperature/pH extremes [7,8]). Pitting prevalence may also be positively correlated with surface precipitate abundance [7], with pits potentially forming preferentially around these precipitates.

Many mechanisms of pit formation have been proposed. Initially it was thought that pits form due to either mechanical removal or dissolution of individual spheres ('globules') in the glass structure [11]. More commonly, analogies to the metallurgical theory of 'pitting corrosion'

* Corresponding author.
E-mail address: r.hand@sheffield.ac.uk (R.J. Hand).
[1] Now at EDF, Hinkley Point Visitor Centre, Cannington Court, Church Street, Bridgwater, Somerset, TA5 2HA.

https://doi.org/10.1016/j.jnoncrysol.2023.122230
Received 22 November 2022; Received in revised form 8 January 2023; Accepted 16 February 2023
Available online 11 March 2023

are drawn, where selective attack begins at a scratch, lattice defect, or compositional heterogeneity [18]. This generates a cavity with a geometry that slows diffusion to and from the defect site, accelerating its further dissolution/deepening as a highly aggressive local chemistry develops at its tip [18]; in the case of silicate and borosilicate glasses this would be a highly alkaline environment [7,19].

2.2. Extended or "vermiform" features

Extended tube-like or "vermiform" features have been observed by a range of authors (see, for example, [10,16,20–22]). When viewed in cross section, the features in question are curvilinear in nature with cross-sectional diameters of the order of micrometres; originating on the glass surface (noting that the original glass surface may no longer be present) and penetrating down into the bulk glass a distance of a few to tens of micrometres, before terminating in a rounded fashion. These features may be hollow or filled and, as shown in Fig. 1, can be distinguished from fractures given their smoothly curved non-angularity and rounded (high radius) termination.

Features of this type have been given a range of names in the literature including asperities [20], channels [21], chemiturbation channels [10], curved-branched irregular micropits [22], etch planes [16], grooves [20], longish structures [23], putative endolithic microborings [24], troughs [21], tubular structures [25], tunnels [26,27], and wormholes [28]. Given the features may be hollow or filled we use the term "vermiform" to describe them in the following.

As well as the vermiform features two types of cracks can be observed in Fig. 1. Namely ones containing alteration layers and very narrow cracks that do not contain alteration layers. In both cases the cracks have sharp terminations. The cracks that do not contain alteration layers are believed to have formed post-test during sample sectioning and/or dehydration in the electron microscope vacuum.

The origin of vermiform features is widely debated. Given the features resemblance to biologically formed structures, their biogenicity is often claimed, with colonising microbes able to form features with these morphologies by continuously excreting substances like acids, chelating agents and enzymes which dissolve the glass [15]. Why microorganisms evolved to do this is debated, with the main theories [29] including reasons of nutrient acquisition or protection (from physical extremes, predatory grazing, substrate detachment, or the potential for mineralisation). A number of criteria have been suggested to evaluate whether a biological origin is possible, including the geological/experimental context, the morphology of the feature and any geochemical evidence. Whilst some authors only consider biotic generation mechanisms [16,30], others state that such features have never been recreated in laboratory experiments, even *via* biological mechanisms [31–33].

Abiotic formation mechanisms typically postulate that vermiform features result from preferential dissolution of a precursor feature. The precursor feature may be structural, morphological, chemical or a combination of these. Both pits and more extended features could potentially result from preferential dissolution at micro-heterogeneities such as alkali-rich areas [8,34–36] or phase-separated components; an extreme example being the acid removal of the sodium borate rich phase from Vycor glass (see, for example, [37]). The modifier-rich percolation channels postulated in the modified random network model of glass structure [38], and which have been inferred in some high level waste glasses [39,40] also provide potential sites for preferential ion exchange resulting in a localised pH increase and accelerated attack. In addition to possible percolation channels, all glasses inherently contain more highly strained bonds due to their amorphous nature and variable bond angles that could act as potential sites for chemical attack. Preferential dissolution around physically damaged sites is also possible, with stress corrosion assisted growth of cracks being well known (see, for example, [41,42]); stress corrosion assisted fracture has been postulated to occur during the leaching of glass powders [43]. Surface roughness has also been shown to influence the development of alteration layers [20] and pit coalescence has been suggested as a cause of more extended features [44]. In addition, pre-existing contamination (*e.g.* dirt, finger grease *etc.*) may also provide preferential sites for corrosion [45,46], however adequate sample washing should prevent this in laboratory experiments.

Aside from formation *via* dissolution [16], other potential abiotic causes include burial metamorphism of organic matter or un/misidentified ambient inclusion trails (AITs) formed as mineral inclusions forcibly migrate through a material with enough force and energy to erode a hollow tubular structure [31,47]. These can often be excluded where the diagnostic features (a terminal crystal and longitudinal striae) are missing [23,48]. None of these mechanisms are relevant to laboratory-dissolved crystal-free glasses. Similarly, although some authors [49] have interpreted morphologically similar features to be

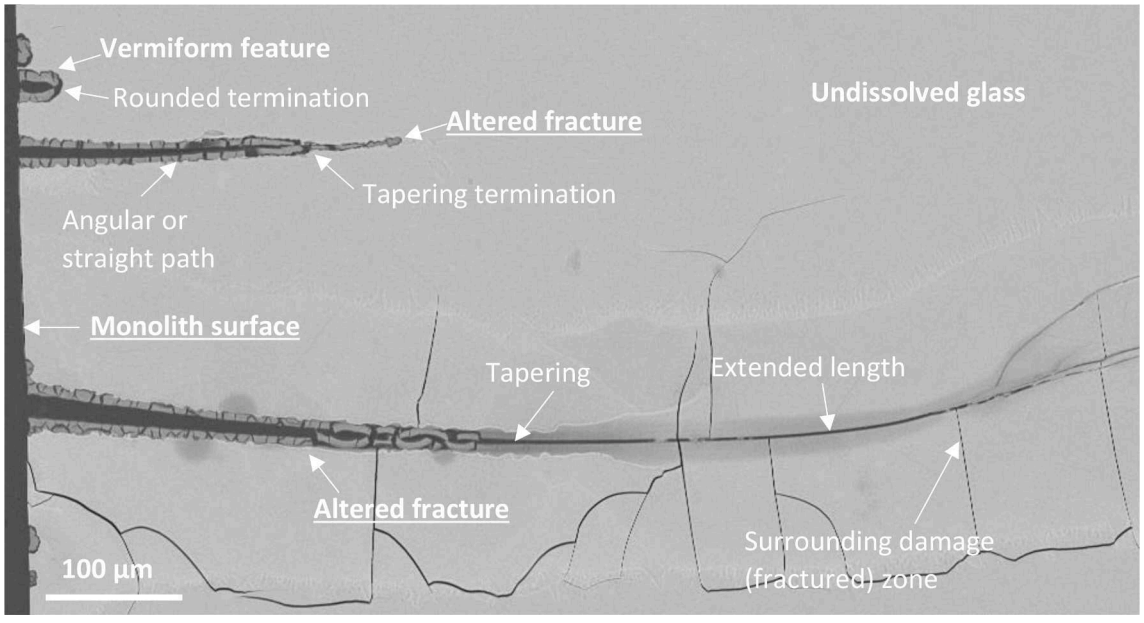

Fig. 1. Scanning electron microscope image illustrating differences between vermiform features and dissolved fractures in a monolith cross-section of the international simple glass (ISG) after 672 d dissolution at 90 °C in ultra-high quality water. Micrograph from current work – full experimental details are given below.

microcracks [33]; cracks can be distinguished on the basis of either their sharp pointed terminations or their extension from one side of the sample to the other.

Despite there being more studies conducted on abiotic glass alteration than biotic [50], the reverse appears to be the case when analysing specific features. Further experiments are needed to explore the abiotic explanations [24,51], and to quantify their effect on the long term durability of glass wasteforms [10], especially as such features have been reported to increase both dissolution rates [52] and glass surface areas by 240% [53]. Understanding how features may be formed abiotically is relevant to earth sciences, palaeontology, biological sciences, material science [54] and even interplanetary science, given that subaqueous basaltic glass alteration on Mars has been postulated to involve both abiotic and biotic processes [55].

Thus to gain greater understanding of how vermiform features develop in an abiotic context this work characterises the features generated during accelerated monolith dissolution testing of basaltic and analogue high level waste (HLW) glasses. Comparisons are drawn between the features generated on each glass type, before the impact of these features on surface areas is quantified and their potential formation mechanisms discussed.

3. Experimental

3.1. Materials

3.1.1. Basaltic glasses and MW25 glass

Three basaltic glasses based on the composition given by Techer et al. [56], with fixed total alkaline earth contents, but with varying quantities of magnesia and lime, were prepared from batched mixtures of high quality glass making sand (Loch Aline; 99.5%), sodium carbonate (Sigma Aldrich; 99.9%), calcium carbonate (Sigma Aldrich; 99.9%), potassium carbonate (Alfa Aesar, 99%), hydrated magnesium carbonate (Fisher, 99%), aluminium trihydroxide (Sigma Aldrich, 99%), ammonium dihydrogen phosphate (Alfa Aesar, 98%), titanium dioxide (Sigma Aldrich, 99.8%), strontium nitrate (Aldrich, ≥98%), lithium carbonate (Alfa Aesar, 99%), iron (III) oxide (Alfa Aesar, 98%) and manganese (II) carbonate (Alfa Aesar, 99.8%). These glasses were prepared as part of a larger series examining the effect of magnesia and lime on the durability of basaltic glasses [57].

An inactive analogue of a UK 25 wt% waste loaded MW glass (MW25) was prepared from an alkali borosilicate base glass 'frit' (MW0.5Li which contains half the required lithium) and a simulated Magnox waste 'calcine' (WRW17), both provided by the National Nuclear Laboratory. Lithium carbonate was used to bring the lithium content up to the full required quantity.

The glasses were produced by heating the batched materials at 1450 °C (basaltic compositions) or 1050 °C (MW25) in a platinum-rhodium crucible. Each composition was melted for a total of 5 h in an electric furnace with 1 h to form a batch free melt followed by 4 h stirring. The melts were cast into pre-heated iron moulds and then annealed at 670 °C (basaltic glasses) or 500 °C (MW25) for 1 h. After annealing the glass ingots were furnace cooled to room temperature. Following an HF digest inductively coupled plasma-optical emission spectroscopy (ICP-OES) was used to determine unaltered glass compositions (see Table 1).

Table 1
Measured and normalised compositions (ICP-OES) in mol% of the laboratory made basaltic glasses and MW25 glass studied here. Others for MW25 are all present at < 1 mol% oxide level. Errors are estimated to be ± 1% for major oxides and ± 5% for minor oxides.

Oxide	Oxide mol% measured			
	0Ca100Mg	50Ca50Mg	100Ca0Mg	MW25
Al_2O_3	9.13	7.62	7.90	2.56
B_2O_3	0.00	0.00	0.00	17.57
CaO	0.36	11.80	24.8	0.24
Fe_2O_3	4.56	4.56	4.51	1.56
Li_2O	1.81	1.81	1.78	6.93
MgO	23.44	14.13	0.00	7.83
MnO	0.16	0.16	0.15	0.00
Na_2O	3.08	3.26	3.05	9.02
P_2O_5	0.08	0.09	0.12	0.08
SiO_2	55.50	54.70	55.86	50.14
SrO	0.35	0.36	0.34	0.18
ZrO_2	0.00	0.00	0.00	0.67
TiO_2	1.53	1.51	1.49	0.00
Others	–	–	–	3.22
Total	100.00	100.00	100.00	100.00

3.1.2. International Simple Glass (ISG)

Samples were prepared from two annealed 500 g blocks (Lot L12012601-M12042001 and Lot L12012601-M12042501) of the International Simple Glass (ISG) [58,59] provided by the International Glass Corrosion Working Group.

3.2. Durability testing

Durability testing was conducted using the ASTM MCC-1 [60] protocol. The glass ingots were cut into ~10×10×5 mm monoliths, progressively ground and polished using P600, P800 and P1200 grit SiC abrasive papers and then 6, 3 and 1 μm oil based diamond suspensions. The polished monoliths were sequentially cleaned using ultra high quality (UHQ) water and isopropanol before drying at 90 °C for ~ 12 h. Prepared monoliths were placed into clean Savillex 60 ml perfluoralkoxy (PFA) Teflon standard vessels containing a support screen ('basket') of the same material. Ultra High Quality (UHQ, 18 MΩ cm) water was added in appropriate quantities to these vessels to give a sample surface area to volume of attacking solution (SA/*V*) of 10 m^{-1}; the required leachant volume for each timestep was calculated based on the average geometric surface area measured for all monoliths of a given timestep. The sealed vessels were placed into a GenLab MINO/40 oven at 90 ± 2 °C for 28, 56, 112, 224, 461 (0Ca100Mg, 100Ca0Mg, MW25 and ISG) or 468 (50Ca50Mg), and 672 d. After testing the vessels were removed from the oven, weighed and allowed to cool to room temperature before the monolith was removed and allowed to air-dry for 24–48 h; chemical analysis of the leachates was also undertaken but is not the focus of the work reported here and is reported elsewhere [57].

For examination, the dried monoliths were lifted from their support screens, using soft plastic tweezers; some localised damage to alteration layers during this process, restricted to the area in contact with tweezers, was unavoidable. Two of the triplicate monoliths per composition/timestep were placed into plastic sample clips before being mounted in an epoxy based mounting resin (80% Buehler EpoxiCureTM 2 Epoxy Resin thoroughly mixed with 20% Buehler EpoxiCureTM 2 Epoxy Hardener). The epoxy-mounted samples were successively ground and polished to a 1 μm finish using P600, P800 and P1200 grit SiC abrasive papers with isopropanol as a lubricant and then 6, 3 and 1 μm oil based diamond suspensions. For scanning electron microscopy (SEM) copper-tape was applied to electrically connect the bottom and top of the resin-mounted samples which were then carbon-coated using a Quorum Q150T ES Plus.

3.3. Scanning electron microscopy

To identify localised alteration features polished cross sections of the MCC-1 samples were characterised with a Hitachi TM3030 Plus scanning electron microscope (SEM) coupled with Bruker Quantax 70 energy

dispersive spectrometer (EDS). An accelerating voltage of 15 kV and a beam current of 2×10^{-9} A was used with a working distance of 7–9 mm. EDS spectra were collected for at least ten minutes, with back-scattered electron (BSE) images collected at the maximum available resolution.

3.4. DNA assay

Aliquots of unacidified MCC-1 leachate aliquots leachates from 2 experiments that had yielded significant vermiform features (0Ca100Mg basaltic glass dissolved for 461 days and ISG dissolved for 224 days) were analysed for the presence of DNA *via* a Quant-iT™ PicoGreen™ dsDNA Assay test. The leachates were tested and analysed in three forms: (1) without further processing, (2) after they had been concentrated and (3) after attempts were made to extract genomic DNA (gDNA) *via* the EtNa protocol [61].

4. Results

4.1. Basaltic glasses

Vermiform features were observed on all basaltic glass compositions, with no noted compositional dependencies or differences across the different glasses. On each analysed cross section (~28 mm perimeter), 50 to 300 features were observed scattered randomly across the surface, with no evidence of abundance consistently varying with dissolution duration. Morphologies varied from the comparatively simple (see Fig. 2) to the complex (see Fig. 3), with some evidence of increasing feature complexity with dissolution duration, but no obvious correlation with glass durability.

The simple solitary vermiform features, typically penetrating the glass at angles of ~ 90° (Fig. 2a and c), but not always (Fig. 2b, d and e), are the most abundant type in all basaltic glasses at all dissolution durations. Solitary features were 2–60 μm in length, with a width that is typically a factor of 2 – 4 times the thickness of the alteration layer on the surface of the glass. These features often have relatively straight paths (Fig. 2a and c–e) but smooth curvilinear forms are also seen (Fig. 2b). In general, these simple vermiform features contain both a narrow void (comparable to that which separates the glass alteration layer from the sample elsewhere, thought to be an artefact of cross-section preparation and SEM examination) and material resembling the alteration layer on the glass surface. As shown in Fig. 2 they also contain a notably distinct central zone, no more than 0.5 μm in width, of 'bright', higher atomic number material, in BSE images. The central zone is too small to reliably measure *via* EDS however it is likely iron rich.

More complex features can be categorised as 'clusters' of 5–20 closely spaced features over a small distance (Fig. 3a–c); multiple features emanating from a single near-surface region (Fig. 3d–g); and branching after extension into the sample (Fig. 3h–j). Other more complex features such as the spiralling central thread were occasionally seen (Fig. 3k and l).

4.2. MW25

Samples of MW25 showed a similar range of vermiform features to the basaltic glasses, although they are coupled with a more complex series of layers on the glass surface. Fig. 4 shows solitary simple features that are essentially similar to those seen in Fig. 2; however, they often lie below an outermost layer of altered material (most clearly seen in Fig. 4c). Although they are observed at all dissolution durations and appear unchanged with duration, these features appear less often than in the basaltic glasses with a frequency of 10–25 per cross-sectional perimeter (28 mm) compared to 50–300 per cross-sectional perimeter for the basaltic glasses. They also tend to be somewhat shorter on average, being 3–15 μm in length rather than 3–60 μm. As with the basaltic glasses these features typically penetrate the surface at angles of 90° (Fig. 4b and c) but lower angles are also seen (Fig. 4a). Once again a thin brighter strand can be seen down their centre although the contrast is less marked than in basaltic glasses (compare Figs. 4 and 2). A notable difference from the basaltic glasses is the layer of altered material (darker in the image than the unaltered glass) that surrounds these features.

In some cases features show more complex morphologies, for example, branching or sudden changes in direction (Fig. 5a–d) and, in one instance, a clustering of ~ 15 small features ~ 1 μm length was observed over a (cross sectional) distance ~ 35 μm (Fig. 5e). Complex features were also seen at sample corners (Fig. 5e and in one case extended ~ 100 μm into the glass (Fig. 5f).

4.3. ISG

Comparable, but not identical, features are also observed on dissolved ISG samples. Fig. 6 shows single solitary features, which are again the most abundant type of features (at 10–30 occurrences per monolith cross section). These penetrate further into the monoliths than in MW25 but far less than in the basaltic glasses (3–40 μm compared to 3–15 μm and 3–60 μm, respectively), again not obviously correlated with relative durability. Unlike the equivalent features in both the basaltic glasses and MW25, the 5 μm width of these features is not entirely filled by alteration layers, with the majority of the vermiform feature being an unfilled void (see Fig. 6). The outermost alteration layer lines the edges of these features but is often fractured, although this may be an artefact associated with sample preparation and SEM imaging; breakage is nearly always observed at the feature tip. As with MW25 an inner alteration layer appears displaced inwards by the vermiform features, effectively "bulging" inwards in order to maintain a consistent layer thickness. Vermiform features never cross-cut this layer.

Branching of vermiform features is again seen (Fig. 7), however the point of bifurcation is always at the surface for ISG unlike the other glasses studied (compare Fig. 7 with Figs. 3h–j and 5a,b,d). Localised feature clustering was not observed for ISG.

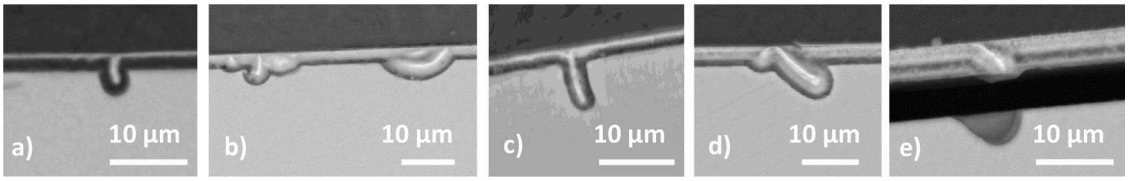

Fig. 2. SEM-BSE images of typical simple vermiform features observed on basaltic glasses (a) 100Ca0Mg after 28 d; (b) 0Ca100Mg after 56 d; (c) 50Ca50Mg after 112 d; (d) 100Ca0Mg after 461 d and (e) 50Ca50Mg after 672 d dissolution. In all images unaltered glass is at the bottom of the image and the dark region at the top of each image is the mounting resin.

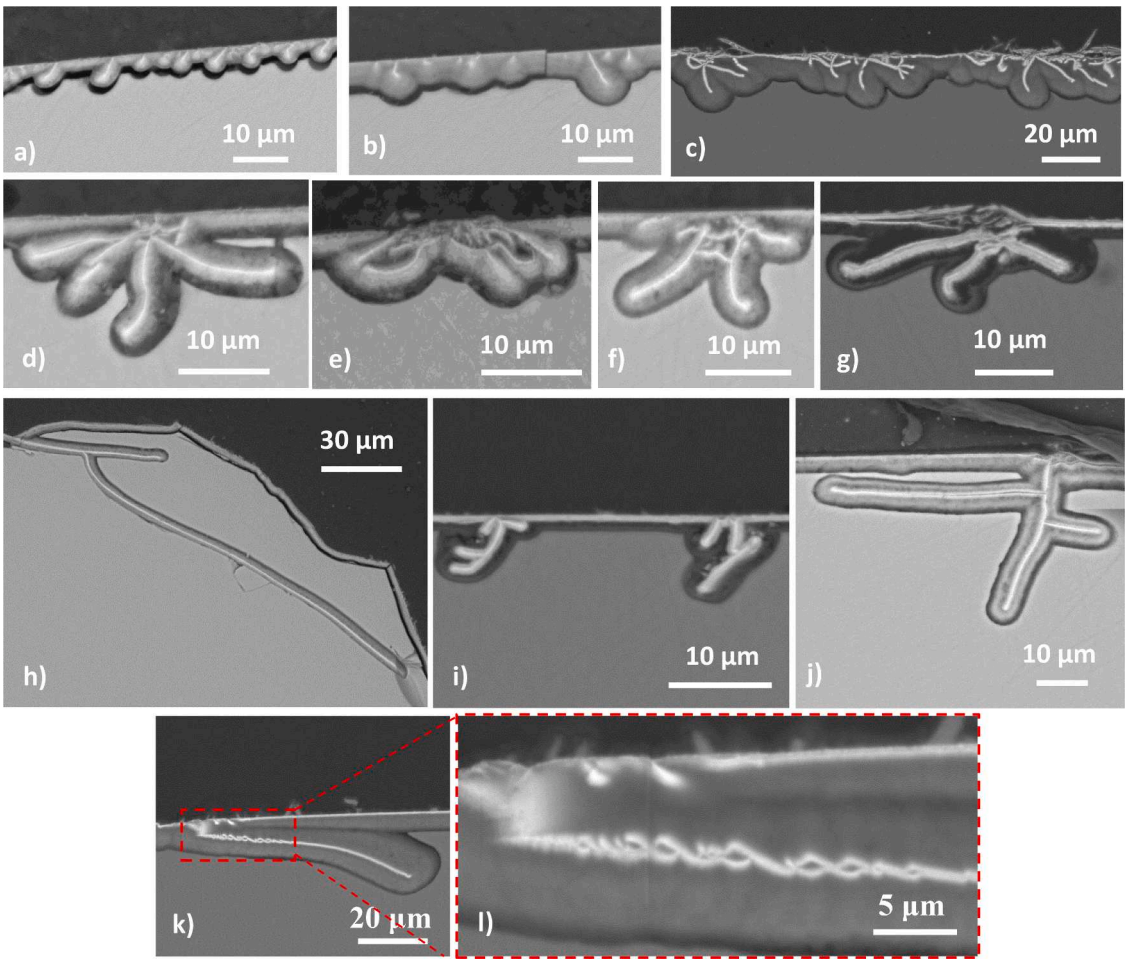

Fig. 3. SEM-BSE images showing clustering of vermiform features in (a) 50Ca50Mg after 56 d, (b) 0Ca100Mg after 112 d, (c) 0Ca100Mg after 461 d; multiple features extending from a single origin in (d) 50Ca50Mg after 56 d, (e) 50Ca50Mg after 112 d, (f) 50Ca50Mg after 461 d, (g) 100Ca0Mg after 461 d; and branching in (h) 0Ca100Mg after 224 d, (i) 100Ca0Mg after 461 d and (j) 50Ca50Mg after 468 d; (k) a complex spiral feature in 0Ca100Mg after 461 d enlarged in (l). In all images unaltered glass is at the bottom of the image and the dark region at the top of each image is the mounting resin.

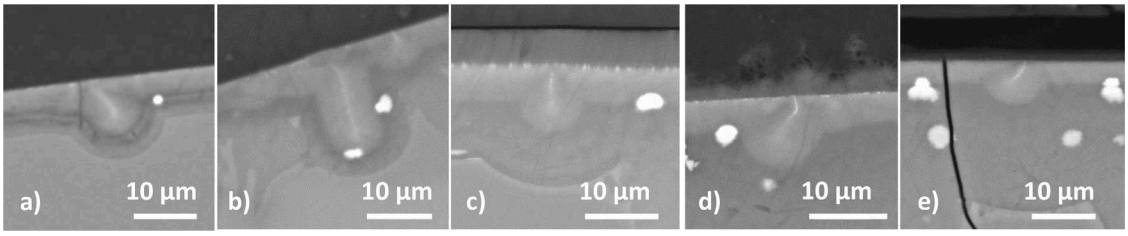

Fig. 4. SEM-BSE images of simple solitary vermiform features formed on MW25 samples after (a) 28 d, (b) 56 d, (c) 224 d, (d) 468 d and (e) 672 d dissolution. In all images unaltered glass is at the bottom of the image and the dark region at the top of each image is the mounting resin.

4.4. DNA assay

No detectable DNA was identified in the two leachates analysed. The detection limit is ~ 5–200 million cells per millilitre.

5. Discussion

Vermiform features have been observed across all glasses studied at all time periods with only limited evidence of any time dependence after the initial 28 d of the test. Their detailed nature varies with glass composition with the basaltic glasses appearing to contain more vermiform features, which can be significantly longer and show more evidence of complexity compared to MW25 and ISG. The features in both the basaltic glasses and MW25 are filled with an alteration layer including a central region enriched in higher atomic number elements, whereas the features in ISG are unfilled.

5.1. Biotic origins

Vermiform features are often considered to have a biotic origin hence we consider that possibility here. No biological materials were added to the experimental vessels, which went through a thorough cleaning process (an in-house version of the procedure detailed in [62]) before use. The experiments were run in a clean, but non-sterile, laboratory environment. All reagents and solutions were laboratory grade and were stored appropriately to minimise the likelihood of biological influence.

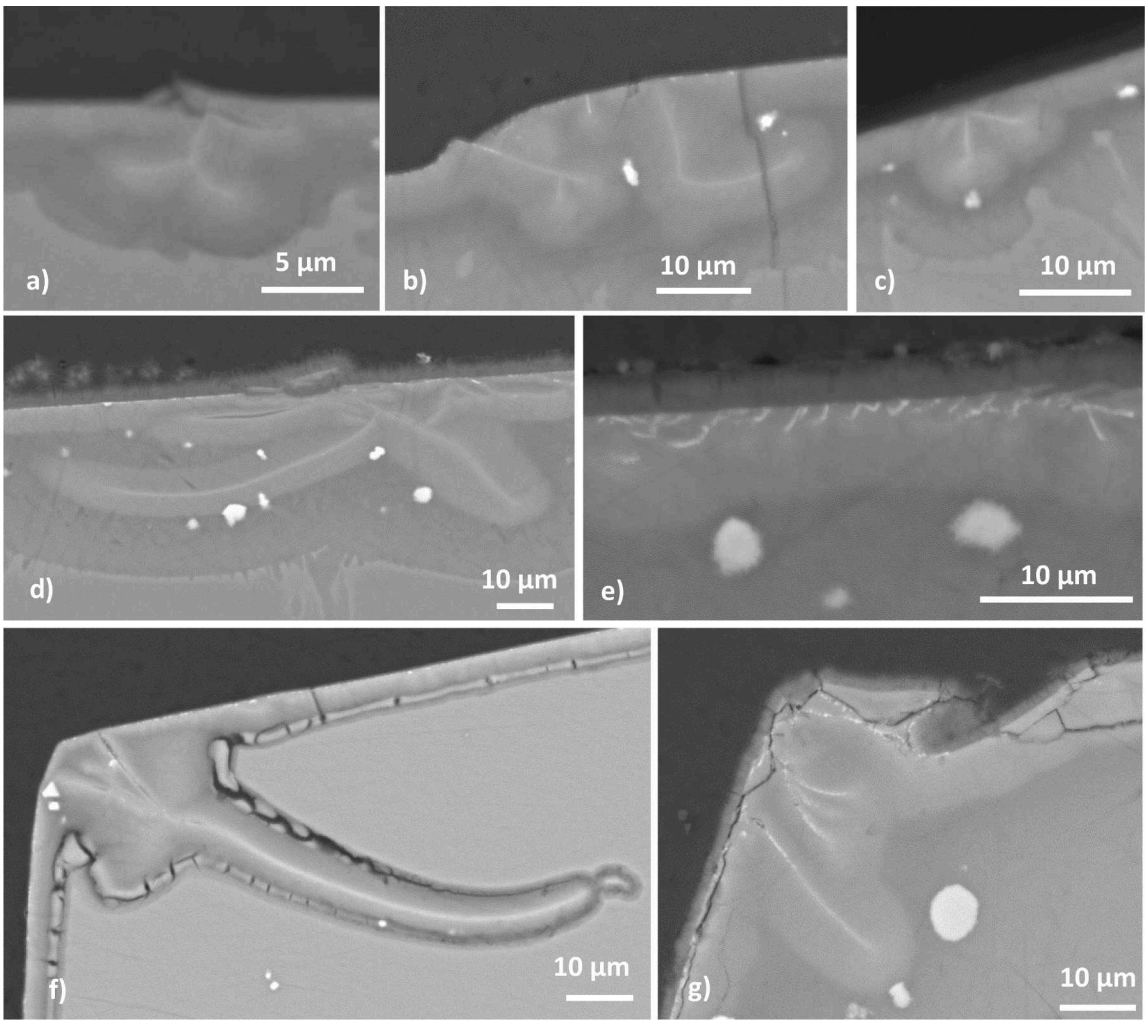

Fig. 5. SEM-BSE images of complex vermiform features formed on MW25 samples showing features branching, changing course and clustering after (a) 28 d; (b) & (c) 56 d; (d) & (e) 468 d and formed at sample vertices after (f) 28 d and (g) 224 d dissolution. In all images unaltered glass is at the bottom of the image and the dark region at the top of each image is the mounting resin.

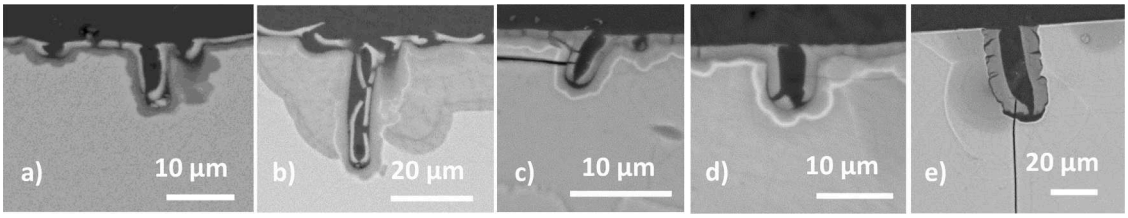

Fig. 6. SEM-BSE images of simple solitary vermiform features formed on ISG samples after (a) 28 d, (b) 56 d, (c) 224 d, (d) 468 d and (e) 672 d dissolution. In all images unaltered glass is at the bottom of the image and the dark region at the top of each image is the mounting resin.

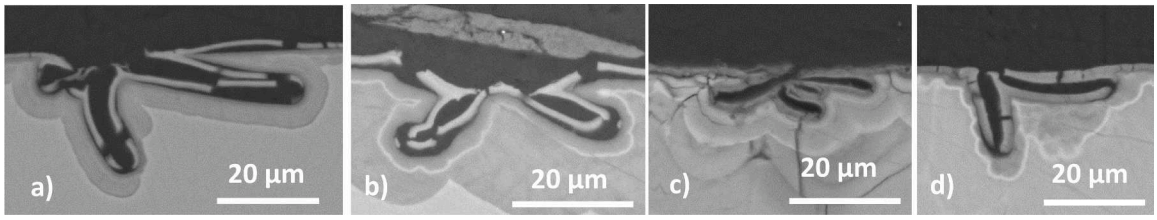

Fig. 7. Branching of vermiform features in ISG after (a) 28 d, (b) 56 d, (c) 224 d and (d) 468 d.

During the 90 °C MCC-1 test the pH of the leachant in each vessel increased to ~ 8.5–9.5. For the two leachants assayed after testing, the DNA assays resulted in no evidence of DNA in the vessels. Furthermore it has been suggested that any biological process involving microbes excreting glass dissolving substances would be near-impossible to see in the laboratory due to the unavoidable slowness of such processes [15]. Overall it is therefore considered to be highly unlikely that the features observed in these tests have a biotic origin.

5.2. Abiotic origins

Abiotic mechanisms require preferential dissolution around a structural/chemical or, morphological precursor. Potential structural precursors include strained bonds in the glass network, nano-heterogeneities or phase separated regions. Strained bonds necessarily must exist in glasses due to the variable ring sizes seen in network glass structures. While these would provide very localised sites for initial attack, a number of such sites would probably need to be adjacent to act as a precursor site for the growth of extended feature. Nano-heterogeneities such alkali-rich channels could also provide a starting point for localised attack and have previously been suggested as the origin of strength controlling Griffith flaws in silicate glasses [63] or features along which cracks could propagate [64]. Borosilicate glasses (MW25 and ISG) are widely thought to contain borate and silicate sub-networks, however, no evidence of larger scale phase separation or compositional variation was noted in any of the glasses studied during pre-dissolution characterisation *via* SEM-EDS; in addition the transmission electron microscope data in the literature indicate that ISG is not phase separated [59].

Morphological precursors are also possible; the samples were finished to a mirror-like (1 μm) surface finish but finer scale features could have remained on the sample surface. It has been shown that the smoothest surfaces on ISG are produced by a surface melting technique [59,65], although this also resulted in some compositional modification. In the current work there was some limited evidence of increased vermiform feature abundance at monolith corners where preparation-induced damage is likely to be greatest; chipping of corners during sample production resulting in unusable monoliths was an issue during sample preparation. The polished glass monoliths were not re-annealed after polishing and hence some residual stresses, introduced by the cutting, grinding and polishing processes, may be present in the glass surfaces. Any localised tensile residual stresses could potentially accelerate the localised extension of morphological damage *via* stress corrosion [41]. Furthermore the chemistry and pH of leachant in scratches/cracks is likely to change more rapidly during glass dissolution than the bulk fluid and may thus promote vermiform feature development [20,43]. Regions with larger amounts of morphological damage arising from sample preparation may also explain the clustering of features observed in the basaltic glasses and MW25.

Even the simplest single vermiform features were, on occasion, noted to have sinuous curvilinear paths. This may be associated with the lack of long-range order in glasses: preferential attack of locally strained bonds may divert the course of the vermiform features, although a number of such sites would probably need to be adjacent to cause such deviation. The lack of long-range order in glasses means there are no structural elements that could preferentially dissolve to produce the straight features seen in dissolution of crystalline materials [66].

More complex features such as the helicoidal structures shown in Fig. 3k and l have previously been used as strong evidence of biological causes [67], as such morphologies are commonly associated with living cells [68]. However, helical forms can also be generated *via* abiotic processes. For example, helical AITs (see also Section 2.2), formed by the propulsion of mineral crystals through a matrix, have previously been reported [47,69]. Dohmen et al. identified a similar feature in some glass dissolution experiments on U-bearing soda-lime-silica glass beads, which they attributed to pH fluctuations resulting in gel shrinkage and crack generation [70].

The filled features seen in the basaltic glasses and MW25 usually had a central region which elemental contrast indicates has a higher atomic number (Z), and are apparently iron rich, although the features were not large enough to enable definitive identification. Iron rich particles have been previously reported in alteration layers in both laboratory and environmentally altered samples [9]. Such variation in composition indicates locally variable solution chemistry as the vermiform features develop.

Overall it seems most likely that the vermiform features develop from damage sites arising during monolith preparation. Both the presence of precursor cracks, and residual stresses arising from grinding and polishing, could promote localised chemical attack. The residual stress distribution and naturally strained bonds in the glass structure may impact the direction of crack growth.

5.3. Vermiform features and glass dissolution

The formation of vermiform features is likely coupled with alteration layer formation. Dissolution of vermiform features likely provides elements for alteration layer formation, but alteration layer formation may also infill (as seen in both the basaltic glasses and MW25 – see Figs. 2–5) and thus reduce the effect of vermiform features, potentially also 'protecting' them from further growth.

Large numbers of vermiform features could potentially result in an increase in the effective surface area. To obtain an estimate of the scale of this effect we consider the monolith cross sections to be representative of a ~ 2 μm thickness through the monolith (*i.e.* there are 5000 of these cross sections per monolith) and have modelled all vermiform features as simple uniform cylinders orientated at 90° to the monolith surface (*i.e.* all features are of the simple type with a fixed length). The results are shown in Table 2. It can be seen that the potential increase in surface area is relatively small, although it becomes more significant for the larger numbers of features seen in the basaltic glasses. Once the features have filled with alteration products they would not be expected to influence surface area. Hence it seems likely that these features have limited effect on the total area available for dissolution, even though localised more rapid dissolution must be involved in their creation.

It can be seen from Table 2 that more, and on average, longer features are seen on the basaltic glasses studied. Solution measurements indicate that the basaltic glasses dissolve more slowly than ISG and MW25. After 720 d the normalised mass losses for Si NL_{Si} ~ 2–3 g m^{-2} and Na, NL_{Na} ~ 5–30 g m^{-2} for the basaltic glasses compared with NL_{Si} ~ 10 g m^{-2} (MW25) and 15 g m^{-2} (ISG) and NL_{Na} ~ 120 g m^{-2} (MW25) and 80 g m^{-2} (ISG). This indicates that the glass surface is being removed more rapidly with the ISG and MW25 than with the basaltic glasses, and may therefore explain why the observed features are shorter.

Table 2
Estimated changes in surface area due to vermiform features.

Glass type	Average number of features/ section perimeter	Average feature depth /μm	Typical feature radius /μm	Area associated with one feature /m^2	Percentage increase in surface area
Basaltic	50 - 300	31	1	1.95×10^{-10}	112 - 173
MW25	10 - 25	9	2.5	1.41×10^{-10}	102 - 104
ISG	10 - 30	21.5	2.5	3.38×10^{-10}	104 - 113

6. Conclusions

Locally extended features indicating locally accelerated dissolution were seen on all the MCC-1 samples of 5 different glasses studied. The features were distinguished from cracks by their smoothly curved non-angularity and rounded (high radius) termination and were hollow or filled. Given these observations and the range of names applied to similar features in the literature we have concluded that vermiform most accurately describes these features while not implying a specific mechanism of formation. The features were visible after 28 d and their distribution / frequency did not show a strong dependence on time after that. The number of features depended on glass composition and the nature of their geometry varied with glass composition. Features on basaltic glasses and MW25 were filled and had a central region that was enriched in a higher mass element, likely iron. The majority of features had quite simple geometries but a small number with more complex morphologies were observed on all of the glass types studied here. The location of these features is thought to be most probably linked to residual damage arising from the monolith production providing sites for locally accelerated dissolution; this point could be investigated in future using fire polished samples. Despite being numerous, and sites of localised accelerated dissolution, the impact of these features on the total surface area during dissolution is calculated to be limited. Hence the surface area term used to calculate normalised mass losses and normalised loss rates will not be greatly in error as a result of these features.

CRediT authorship contribution statement

James T. Mansfield: Conceptualization, Investigation, Visualization, Writing – review & editing. **Clare L. Thorpe:** Writing – review & editing. **Claire L. Corkhill:** Supervision, Writing – review & editing. **Mike T. Harrison:** Writing – review & editing. **Hand:** Conceptualization, Supervision, Visualization, Writing – original draft, Writing – review & editing.

Declaration of Competing Interest

The authors declare that they have no known competing financial interests or personal relationships that could have appeared to influence the work reported in this paper.

Data availability

Data will be made available on request.

Acknowledgments

James Mansfield thanks the UK Engineering and Physical Sciences Research Council (EPSRC) and the National Nuclear Laboratory (NNL) for funding as part of the Next Generation Nuclear (NGN) Centre for Doctoral Training programme. We thank Lisa Hollands and Tes Monaghan (both University of Sheffield) for help with glass melting and sample preparation respectively. We thank Victoria Workman and Heather Grievson (both University of Sheffield) for the DNA assays and the ICP analysis respectively. Conversations and guidance from Colleen Mann (University of Sheffield) helped to direct this research and are greatly appreciated. Claire Corkhill acknowledges EPSRC for the award of an Early Career Research Fellowship (EP/N017374/1). Clare Thorpe acknowledges EPSRC for the award of a David Clarke Fellowship (EP/S012400/1). This research utilised the HADES/MIDAS facility [71] at the University of Sheffield established with financial support from EPSRC and BEIS, under grant EP/T011424/1, and the PLEIADES facility, established with financial support from the EPSRC National Nuclear User Facility (EP/V035215/1).

References

[1] C. Thorpe, J. Neeway, C. Pearce, R. Hand, A. Fisher, S. Walling, N. Hyatt, A. Kruger, M. Schweiger, D. Kosson, C. Arendt, J. Marcial, C. Corkhill, Forty years of durability assessment of nuclear waste glass by standard methods, NPJ Mater. Degrad. 5 (2021) 61.
[2] E. Pierce, L. Reed, W. Shaw, B. McGrail, J. Icenhower, C. Windisch, E. Cordova, J. Broady, Experimental determination of the effect of the ratio of B/Al on glass dissolution along the nepheline ($NaAlSiO_4$)–malinkoite (NaBSiO4) join, Geochim. Cosmochim. Acta 74 (2010) 2634–2654.
[3] D. Backhouse, A. Fisher, J. Neeway, C. Corkhill, N. Hyatt, R. Hand, Corrosion of the International Simple Glass under acidic to hyperalkaline conditions, NPJ Mater. Degrad. 2 (2018) 29.
[4] R. Chinnam, P. Fossati, W. Lee, Degradation of partially immersed glass: a new perspective, J. Nuclear Mater. 503 (2018) 56–65.
[5] M.T. Doménech-Carbó, A. Doménech-Carbó, L. Osete-Cortina, M.C. Saurí-Peris, A study on corrosion processes of archaeological glass from the Valencian region (Spain) and its consolidation treatment, Microchim. Acta 154 (2006) 123–142.
[6] M. Gulmini, M. Pace, G. Ivaldi, M. Negro Ponzi, P. Mirti, Morphological and chemical characterization of weathering products on buried Sasanian glass from central Iraq, J. Non Cryst. Solids 355 (2009) 1631, 1621.
[7] J. Mendel, Defense High-Level Easte Leaching Mechanisms program. Final Report, Pacific Northwest Laboratory, Richland, WA, 1984.
[8] A. Fisher, N. Hyatt, R. Hand, C. Corkhill, The formation of pitted reatures on the International Simple Glass during dynamic experiments at alkaline pH, MRS Adv. 4 (2019) 993–999.
[9] S. McLoughlin, R. Hand, N. Hyatt, W. Lee, I. Notingher, D. McPhail, J. Henderson, The long term corrosion of glasses: analytical results after 32 years of burial at Ballidon, Glass Technol. Eur. J. Glass Sci. Technol. A 47 (2005) 59–67.
[10] C. Mann, C. Thorpe, A. Molodowski, L. Field, R. Shaw, L. Boast, R. Hand, N. Hyatt, J. Provis, C. Corkhill, Interactions between simulant vitrified nuclear wastes and high pH solutions: a natural analogue approach, MRS Adv. 2 (2017) 669–675.
[11] H. Staudigel, S. Hart, Alteration of basaltic glass: mechanisms and significance for the oceanic crust-seawater budget, Geochim. Cosmochim. Acta 47 (1983) 337–350.
[12] M. Jercinovic, R. Ewing, Basaltic Glasses from Iceland and the Deep sea: Natural Analogues to Borosilicate Nuclear Waste-Form Glass, University of New Mexico, Albuquerque, 1987.
[13] M. Jercinovic, K. Keil, M. Smith, R. Schmitt, Alteration of basaltic glasses from north-central British Columbia, Canada, Geochim. Cosmochim. Acta 54 (1990) 2679–2696.
[14] I. Thorseth, T. Torsvik, V. Torsvik, F. Daae, R. Pedersen, Diversity of life in ocean floor basalt, Earth Planet. Sci. Lett. 194 (2001) 31–37.
[15] H. Staudigel, H. Furnes, N. McLoughlin, N. Banerjee, L. Connell, A. Templeton, 3.5 billion years of glass bioalteration: volcanic rocks as a basis for microbial life? Earth-Sci. Rev. 89 (2008) 156–176.
[16] M. Fisk, J.L. Crovisier, J. Honnorez, Experimental abiotic alteration of igneous and manufactured glasses, Comptes Rendus Geosc. 345 (2013) 176–184.
[17] C. Kruber, I. Thorseth, R. Pedersen, Seafloor alteration of basaltic glass: textures, geochemistry,and endolithic microorganisms, Geochem. Geophys. Geosyst. 9 (2008) Q12002.
[18] G. Frankel, Pitting corrosion of metals: a review of the critical factors, J. Electrochem. Soc. 145 (1998) 2186–2198.
[19] C. Lenting, O. Pluemper, M. Kilburn, P. Guagliardo, M. Klinkenberg, T. Geisler, Towards a unifying mechanistic model for silicate glass corrosion, NPJ Mater. Degrad. 2 (2018) 28.
[20] L. Sessegolo, A. Verney-Carron, P. Ausset, M. Saheb, A. Chabas, Effect of surface roughness on medieval-type glass alteration in aqueous medium, J. Non Cryst. Solids 505 (2019) 260–271.
[21] A. Fisher, Dissolution of UK vitrified high-level radioactive waste containing zinc and calcium, PhD thesis, University of Sheffield, 2020. pp 97-98,133-135, 272-274. https://etheses.whiterose.ac.uk/29156/.
[22] M. Garcia-Vallès, D. Gomeno-Torrente, S. Martínez-Manent, J. Fernández-Turiel, Medieval stained glass in a Mediterranean climate: typology, weathering and glass decay,and associated biomineralization processes and products, Am. Mineral. 88 (2003) 1996–2006.
[23] S. Dultz, J. Boy, C. Dupont, M. Halisch, H. Behrens, A.-.M. Welsch, M. Erdmann, S. Cramm, G. Helsch, J. Deubener, Alteration of a submarine basaltic glass under environmental conditions conducive for microorganisms: growth patterns of the microbial community and mechanism of palagonite formation, Geomicrobiol. J. 31 (2014) 813–834.
[24] N. McLoughlin, M. Brasier, D. Wacey, O. Green, R. Perry, On biogenicity criteria for endolithic microborings on early earth and beyond, Astrobiology 7 (2007) 10–26.
[25] N. Banerjee, A. Simonetti, H. Furnes, K. Muehlenbachs, H. Staudigel, L. Heaman, M. Van Kranendock, Direct dating of Archean microbial ichnofossils, Geology 35 (2007) 487–490.
[26] R. Mitchell, J. Cuadros, S. Pressel, C. Mavris, D. Sykes, J. Najorka, G. Edgecombe, P. Kenrick, Mineral weathering and soil development in the earliest land plant ecosystems, Geology 44 (2016) 1007–1010.
[27] R. Mitchell, C. Strullu-Derrien, P. Kenrick, Biologically mediated weathering in modern cryptogamic ground covers and the early Paleozoic fossil record, J. Geol. Soc. Lond. 176 (2019) 430–439.
[28] P. Heath, Alternative processing methods for the thermal treatment of radioactive wastes, Sheffield: PhD thesis, University of Sheffield, 2015. pp 183, 211-213. https://etheses.whiterose.ac.uk/9674/.

[29] C. Cockell, A. Herrera, Why are some microorganisms boring? Trends Microbiol. 16 (2008) 101–106.
[30] H. Furnes, H. Staudigel, I. Thorseth, T. Torsvik, K. Muehlenbachs, O. Tumyr, Bioalteration of basaltic glass in the oceanic crust, Geochem. Geophys. Geosyst. 2 (2001), 2000GC000150.
[31] K. Lepot, K. Benzerara, P. Philippot, Biogenic *versus* metamorphic origins of diverse microtubes in 2.7Gyr old volcanic ashes: multi-scale investigations, Earth Planet. Sci. Lett. 312 (2011) 37–47.
[32] I. Thorseth, H. Furnes, O. Tumyr, Textural and chemical effects of bacterial activity on basaltic glass: an experimental approach, Chem. Geol. 119 (1995) 139–160.
[33] K. Benzerara, N. Menguy, N. Banerjee, T. Tyliszczak, G. Brown, F. Guyot, Alteration of submarine basaltic glass from the Ontong Java Plateau: a STXM and TEM study, Earth Planet. Sci. Lett. 260 (2007) 187–200.
[34] C. Jantzen, K. Brown, J. Pickett, Durable glass for thousands of years, Int. J. Appl. Glass Sci. 1 (2010) 38–62.
[35] A. Genga, M. Siciliano, L. Fama, T. Siciliano, A. Mangone, A. Traini, C. Laganara, Characterization of surface layers formed under natural environmental conditions on medieval glass from Siponto (Southern Italy), Mater. Chem. Phys. 2008 (2008) 480–485.
[36] L. Gentaz, T. Lombardo, C. Loisel, A. Chabas, M. Valloto, Early stage of weathering of medieval-like potash–lime model glass: evaluation of key factors, Environ. Sci. Pollut. Res. 18 (2011) 291–300.
[37] A. Varshneya, Fundamentals of Inorganic Glasses: Second Edition, Society of Glass Technology, Sheffield, 2006, pp. 90–92.
[38] G. Greaves, A. Fontaine, P. Lagarde, D. Raoux, S. Gurman, Local structure of silicate glasses, Nature 293 (1981) 611–616.
[39] I. Bardez, D. Caurant, P. Loiseau, N. Baffier, J. Dussossoy, C. Gervais, F. Ribot, D. Neuville, Structural characterisation of rare earth rich glasses for nuclear waste immobilisation, Phys. Chem. Glasses Eur. J. Glass Sci. Technol. B 46 (2005) 320–329.
[40] N. Chouard, D. Caurant, O. Majerus, J.L. Dussossoy, A. Ledieu, S. Peuget, R. Baddour-Hadjean, J.P. Pereira-Ramos, Effect of neodymium oxide on the solubility of MoO3 in an aluminoborosilicate glass, J. Non Cryst. Solids 357 (2011) 2752–2762.
[41] S. Weiderhorn, Influence of water vapor on crack propagation in soda-lime glass, J. Am. Ceram. Soc. 50 (1967) 407–414.
[42] C. Rountree, Recent progress to understand stress corrosion cracking in sodium borosilicate glasses: linking the chemical composition to structural, physical and fracture properties, J. Phys. D Appl. Phys. 50 (2017), 343002.
[43] J. Zhang, J. Neeway, Y. Zhang, J. Ryan, W. Yuan, T. Wang, Z. Zhu, Nanoscale imaging of alteration layers of corroded international simple glass particles using ToF-SIMS, Nuclear Instrum. Methods Phys. Res. Sect. B Beam Interact. Mater. Atoms 404 (2017) 45–51.
[44] W. Geilmann, Contributions to the knowledge of old glasses VI): a peculiar weathering phenomenon on broken Roman glass, Glastechnische Berichte 33 (1960) 291–296.
[45] K. Bange, O. Anderson, F. Rauch, P. Lehuede, E. Radlein, N. Tadokoro, P. Mazzoldi, V. Rigato, K. Matsumoto, M. Farnworth, Multi-method characterization of soda-lime glass corrosion Part 1. Analysis techniques and corrosion in liquid water, Glass Sci. Technol. Glastechnische Berichte 74 (2001) 127–141.
[46] K. Bange, O. Anderson, F. Rauch, P. Lehuede, E. Radlein, N. Tadokoro, P. Mazzoldi, V. Rigato, K. Matsumoto, M. Farnworth, Multi-method characterization of soda-lime glass corrosion. Part 2. Corrosion in humidity, Glass Sci. Technol. Glastechnische Berichte 75 (2002) 20–33.
[47] S. Tyler, E. Barghoorn, Ambient pyrite grains in Precambrian cherts, Am. J. Sci. 261 (1963) 424–432.
[48] N. McLoughlin, D. Fliegel, H. Furnes, H. Staudigel, A. Simonetti, G. Zhao, P. Robinson, Assessing the biogenicity and syngenicity of candidate bioalteration textures in pillow lavas of the ~2.52 Ga Wutai greenstone terrane of China, Chin. Sci. Bull. 55 (2010) 188–199.
[49] J. Crovisier, J. Honnorez, J. Eberhart, Dissolution of basaltic glasses in seawater: mechanism and rate, Geochim. Cosmochim. Acta 51 (1987) 2977–2990.
[50] J. Weaver, P. Depriest, A. Plymale, C. Pearce, B. Arey, R. Koestler, Microbial interactions with silicate glasses, NPJ Mater. Degrad. 5 (2021) 11.
[51] H. Furnes, N. McLoughlin, K. Muehlenbachs, N. Banerjee, H. Staudigel, Y. Dilek, M. de Wit, M. Van Kranendock, P. Schiffman, Oceanic pillow lavas and hyaloclastites as habitats for microbial life through time – a review, in: Links Between Geological Processes, Microbial Activities and Evolution of Life, 4, Springer, 2008. Modern apporaches in Solid Earth sciencesY. Dilek, H. Furnes and K. MuehlenbachsDordrecht.
[52] C. Buckwalter, L. Pederson, G. McVay, The effects of surface area to solution volume ratio and surface roughness on glass leaching, J. Non Cryst. Solids 49 (1982) 397–412.
[53] H. Staudigel, H. Furnes, Microbial mediation of oceanic crust alteration, in: E. Davis, H. Elderfield (Eds.), Hydrogeology of the Oceanic Lithosphere, Cambridge University Press, Cambridge, 2004, pp. 606–624.
[54] J. McCloy, Frontiers in natural and un-natural glasses: an interdisciplinary dialogue and review, J. Non-Cryst. Solids: X 4 (2019), 100035.
[55] N. Banerjee, H. Furnes, K. Muehlenbachs, H. Staudigel, M. de Wit, The potential for early life hosted in basaltic glass on Mars, in: Proceedings of the Second Conference on Early Mars, 2004.
[56] I. Techer, T. Advocat, J. Lancelot, J.M. Liotard, Basaltic glass: alteration mechanisms and analogy with nuclear waste glasses, J. Nuclear Mater. 282 (2000) 40–46.
[57] J.T. Mansfield "Aqueous dissolution of nuclear waste and analogue glasses: dissoluution behavious, surface layers and vermiform features" PhD Thesis, University of Sheffield (2022) pp 83-108. https://etheses.whiterose.ac.uk/31900/.
[58] S. Gin, P. Jollivet, M. Fournier, C. Berthon, Z. Wang, A. Mitroshkov, Z. Zhu, J. Ryan, The fate of silicon during glass corrosion under alkaline conditions: a mechanistic and kinetic study with the International Simple Glass, Geochim. Cosmochim. Acta 151 (2015) 68–85.
[59] T. Kasper, J. Ryan, C. Pantano, J. Rice, C. Trivelpiece, N. Hyatt, C. Corkhill, C. Mann, R. Hand, M. Kirkham, C. Crawford, C. Jantzen, J. Du, X. Lu, M. Harrison, C. Cushman, M. Linford, N. Smith, Physical and optical properties of the International Simple Glass, NPJ Mater. Degrad. 3 (2019) 15.
[60] ASTM C1220-17, "Standard test method for static leaching of monolithic waste forms for disposal of radioactive waste," 2017.
[61] L. Vingataramin, E. Frost, A single protocol for the extraction of gDNA from bacteria and yeast, BioTechniques 58 (2015) 120–125.
[62] ASTM C1285-14, "Standard test methods for determining chemical durability of nuclear, hazardous, and mixed waste glasses and multiphase glass ceramics: the product consistency test (PCT)," 2014.
[63] R. Hand, A. Seddon, An hypothesis on the nature of Griffith's cracks in alkali silicate and silica glasses, Phys. Chem. Glasses 38 (1997) 11–14.
[64] G. Greaves, Exafs for studying corrosion of glass surfaces, J. Non Cryst. Solids 120 (1990) 108–116.
[65] Y. Gong, A. Wren, N. Mellott, Quantitative morphological and compositional laboratory prepared aluminborosilicate glass surfaces, Appl. Surf. Sci. 324 (2015) 594–604.
[66] G. Holdren, R. Bener, Mechanism of feldspar weathering - II Observations of feldspars from soils, Geochim. Cosmochim. Acta 43 (1979) 1173–1186.
[67] N. McLoughlin, H. Furnes, N. Banerjee, K. Moehlenbachs, H. Staudigel, Ichnotaxonomy of microbial trace fossils in volcanic glass, J. Geol. Soc. Lond. 166 (2009) 159–169.
[68] M. Fisk, S. Giovannoni, I. Thorseth, Alteration of oceanic volcanic glass: textural evidence of microbial activity, Science 281 (1998) 978–980.
[69] N. McLoughlin, H. Staudigel, H. Furnes, B. Eickmann, M. Ivarsson, Mechanisms of microtunneling in rock substrates: distinguishing endolithic biosignatures from abiotic microtunnels, Geobiology 8 (2010) 245–255.
[70] L. Dohmen, C. Lenting, L. Fonseca, T. Nagel, A. Heuser, T. Geisler, Pattern formation in silicate glass corrosion zones, Int. J. Appl. Glass Sci. 4 (2013) 357–370.
[71] N. Hyatt, C. Corkhill, M. Stennett, R. Hand, L. Gardner, C. Thorpe, The HADES facility for high activity decommissioning engineering & science: part of the UK national nuclear user facility, IOP Conf. Ser. Mater. Sci. Eng. 818 (2020), 012022.